HHS Public Access

Author manuscript

Cell Rep. Author manuscript; available in PMC 2020 August 13.

Published in final edited form as:

Cell Rep. 2020 July 21; 32(3): 107921. doi:10.1016/j.celrep.2020.107921.

AMPA Receptor Auxiliary Subunit GSG1L Suppresses Short-Term Facilitation in Corticothalamic Synapses and Determines Seizure Susceptibility

Aichurok Kamalova[1,2], **Kensuke Futai**[5], **Eric Delpire**[1,2,4], **Terunaga Nakagawa**[1,2,3,6,*]

[1]Department of Molecular Physiology and Biophysics, Vanderbilt University, School of Medicine, Nashville, TN 37232, USA

[2]Vanderbilt Brain Institute, Vanderbilt University, School of Medicine, Nashville, TN 37232, USA

[3]Center for Structural Biology, Vanderbilt University, School of Medicine, Nashville, TN 37232, USA

[4]Department of Anesthesiology, Vanderbilt University, School of Medicine, Nashville, TN 37232, USA

[5]Department of Neurobiology, Brudnick Neuropsychiatric Research Institute, University of Massachusetts Medical School, Worcester, MA 01605, USA

[6]Lead Contact

SUMMARY

The anterior thalamus (AT) is critical for memory formation, processing navigational information, and seizure initiation. However, the molecular mechanisms that regulate synaptic function of AT neurons remain largely unexplored. We report that AMPA receptor auxiliary subunit GSG1L controls short-term plasticity in AT synapses that receive inputs from the cortex, but not in those receiving inputs from other pathways. A canonical auxiliary subunit stargazin co-exists in these neurons but is functionally absent from corticothalamic synapses. In GSG1L knockout mice, AT neurons exhibit hyperexcitability and the animals have increased susceptibility to seizures, consistent with a negative regulatory role of GSG1L. We hypothesize that negative regulation of synaptic function by GSG1L plays a critical role in maintaining optimal excitation in the AT.

Graphical Abstract

*Correspondence: terunaga.nakagawa@vanderbilt.edu.

AUTHOR CONTRIBUTIONS

T.N. conceived and supervised the project. A.K., E.D., and T.N. designed and conducted experiments. A.K. conducted slice physiology, histology, biochemistry, and behavioral experiments. T.N. conducted outside-out patch recordings. All electrophysiology experiments were conducted at the Nakagawa lab. E.D. provided expertise to generate GSG1L and γ−2 KO mouse lines. T.N. and E.D. generated the targeting construct for GSG1L KO mouse. K.F. provided intellectual and technical expertise in electrophysiology. All authors interpreted the results and analyzed data. T.N. and A.K. wrote the manuscript. All authors edited the manuscript. All authors read and commented on the final manuscript.

SUPPLEMENTAL INFORMATION

Supplemental Information can be found online at https://doi.org/10.1016/j.celrep.2020.107921.

DECLARATION OF INTERESTS

The authors declare no competing interests.

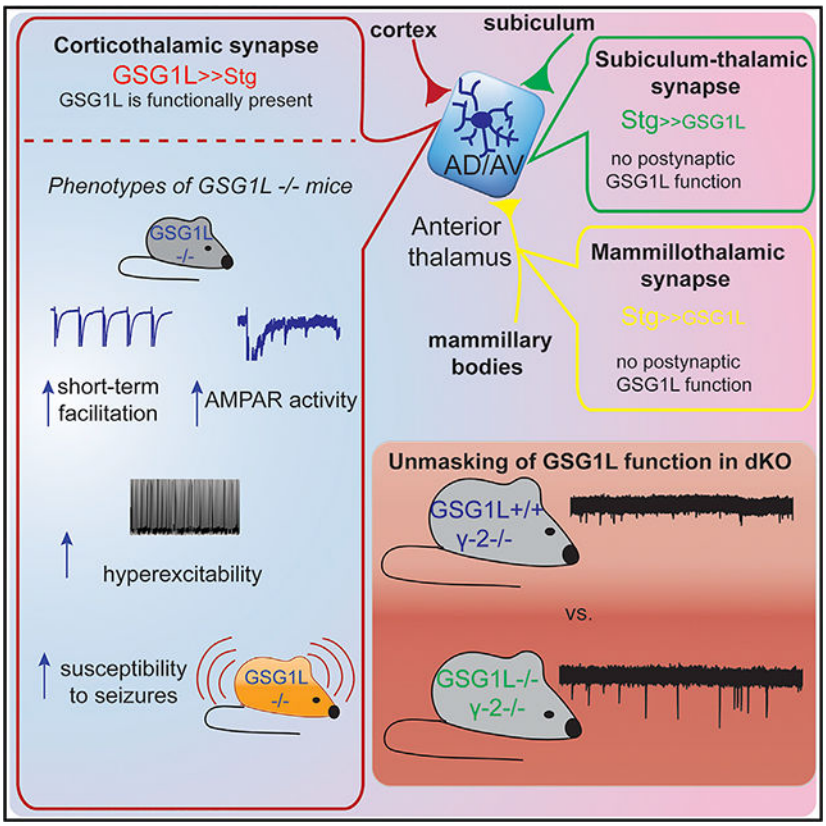

In Brief

Kamalova et al. report the phenotypes of GSG1L KO mice. The synaptic function of AMPAR auxiliary subunit GSG1L in the anterior thalamus is input specific. GSG1L suppresses short-term facilitation and decreases AMPAR activity specifically in corticothalamic synapses, where stargazin is functionally absent. GSG1L KO mice exhibit hyperexcitability and seizure susceptibility.

INTRODUCTION

Regulation of excitatory synaptic transmission is essential for synaptic plasticity, learning, and memory. AMPA-type ionotropic glutamate receptors (AMPARs), which are ligand-gated ion channels activated by the neurotransmitter glutamate, play a key role in this process by mediating most fast excitatory neurotransmission in the brain (Bowie, 2008; Traynelis et al., 2010; Huganir and Nicoll, 2013). GluA1–GluA4 are the pore-forming subunits of AMPARs that assemble into functional ligand-gated ion channels consisting of homo- and heterotetramers (Greger et al., 2017). The canonical structural units of native AMPARs are complexes composed of the core tetramers of GluA subunits and their auxiliary subunits (Nakagawa et al., 2005; Schwenk et al., 2012; Zhao et al., 2019).

AMPAR auxiliary subunits are membrane proteins that regulate ion channel gating and trafficking of AMPARs (Jackson and Nicoll, 2011). The most extensively studied among these are the stargazin/TARPs (transmembrane AMPAR regulatory proteins) (Tomita et al.,

2003). Other auxiliary subunits include cornichon homologs 2 and 3 (CNIH2/3) (Schwenk et al., 2009), CKAMP44 (also known as Shisa9) (von Engelhardt et al., 2010), Shisa6 (Klaassen et al., 2016), SOL-1 (Zheng et al., 2004), and GSG1L (Schwenk et al., 2012; Shanks et al., 2012). Each class of auxiliary subunits is structurally unrelated to the others except for GSG1L and TARPs, which are both claudin homologs. Mod ulation of AMPARs by auxiliary subunits is predicted to substantially affect brain function (Jackson and Nicoll, 2011). Mutations in one or more AMPAR auxiliary subunits lead to neurological and cognitive deficits in both mice and humans (Everett et al., 2007; Hamdan et al., 2011; Floor et al., 2012).

Most AMPAR auxiliary subunits positively modulate AMPAR function by promoting synaptic trafficking and/or modifying gating toward increasing net charge transfer (Jackson and Nicoll, 2011). A subset of auxiliary subunits has mixed effects on gating. For example, CKAMP44 slows AMPAR deactivation, increasing net charge transfer during synaptic transmission, but also delays recovery from desensitization so that the channel is not immediately re-usable (von Engelhardt et al., 2010). Similarly, TARP γ−8 slows AMPAR desensitization and delays recovery from AMPAR desensitization of GluA2 and GluA3 specifically (Cais et al., 2014). Among all auxiliary subunits, GSG1L stands out for having a strong negative modulatory function (McGee et al., 2015; Gu et al., 2016; Mao et al., 2017) (summarized in Figure 1A). Although GSG1L also slows desensitization, it stabilizes the desensitized state (Twomey et al., 2017b) and dramatically delays recovery from desensitization over a magnitude slower than other auxiliary subunits (Schwenk et al., 2012; Shanks et al., 2012). In addition, GSG1L reduces single-channel conductance and calcium permeability of calcium-permeable AMPARs (McGee et al., 2015). Consistently, overexpression of GSG1L decreases the amplitude of evoked excitatory postsynaptic currents (EPSCs) (McGee et al., 2015; Gu et al., 2016; Mao et al., 2017).

Despite its pronounced negative phenotype on AMPAR modulation, GSG1L expression in the brain is low (Schwenk et al., 2014), and it is unclear to what extent it is used *in vivo*. In particular, previous studies using GSG1L knockout (KO) rats reported a modest phenotype in the hippocampus and failed to identify synapses that express the signatures of GSG1L-dependent AMPAR gating modulation, compounded by co-expression of another auxiliary subunit, CNIH2 (Gu et al., 2016).

Here, we demonstrate that GSG1L is enriched in anterodorsal nucleus (AD) and anteroventral nucleus (AV) in the anterior thalamus (AT). The AT is important for memory formation (Aggleton and Brown, 1999; Wolff et al., 2006), encoding head direction information during spatial navigation (Clark and Taube, 2012), as well as seizure initiation and propagation (Mirski and Ferrendelli, 1984; Hamani et al., 2004; Takebayashi et al., 2007; Bittencourt et al., 2010). However, the molecular mechanisms that regulate synaptic function of the AT remain largely unexplored. We find that GSG1L has a postsynaptic role in regulating short-term plasticity in synapses that receive inputs from the cortex, but not from the subiculum or the mammillary bodies (MBs). Furthermore, loss of GSG1L results in increased susceptibility to kai-nate-induced seizures.

RESULTS

GSG1L Is Sufficient to Express Short-Term Plasticity *In Vitro*

The most significant action of GSG1L is the slowing of AMPAR recovery from desensitization (Figure 1A) (Schwenk et al., 2012; Shanks et al., 2012). Therefore, in synapses in which AMPARs desensitize, GSG1L should prevent immediate re-use of AMPARs during repetitive activation and as a result promote short-term depression (STD) or attenuate short-term facilitation. Conversely, elimination of GSG1L should relieve STD or, in an extreme case, convert to short-term facilitation. Consistent with this hypothesis, GSG1L was sufficient to induce STD in a reconstituted system (Figures 1B–1E). Indeed, we found that outside-out patches pulled from HEK293 cells that co-express GSG1L and GluA2 (flip splice variant with unedited Q pore) show significantly depressing currents in response to 1 mM glutamate pulses of 1 ms at 20 Hz, whereas in the absence of GSG1L, the amplitudes remained constant (Figures 1B–1E).

High and Persistent Expression of GSG1L in the AT

We determined the spatiotemporal expression of GSG1L using a transgenic rat that expresses a lacZ reporter under the control of the GSG1L promoter (Figures S1A and S1B). High expression of GSG1L was found in the AT throughout development (Figures 1F and S1C). GSG1L is restricted to AD and AV but absent from anteromedial nucleus (AM) or lateral dorsal nucleus (LD), in agreement with *in situ* hybridization data from the Allen Brain Atlas (Figures 1G, S1D, and S1E) (Lein et al., 2007). AD and AV share progenitor origin (Shi et al., 2017), expression profile of neurotransmitter receptors (Phillips et al., 2019), and afferent and efferent projections (Jankowski et al., 2013). Therefore, we treated the two as a single nucleus, AD/AV, in our investigation. AD/AV receives dense projections from the retrosplenial cortex, the subiculum, and the MB via the mammillothalamic tract (MTT) (Wright et al., 2010) (Figures 1H and 1I). By directly stimulating each afferent, we could selectively record evoked postsynaptic responses from individual inputs (see STAR Methods and Figure 1I) (Petrof and Sherman, 2009; Oh et al., 2014). Analogous to the sensory thalamic relay circuits (Sherman and Guillery, 2004), the inputs to AD/AV neurons are classified into driver and modulator inputs. Specifically, MB inputs drive the firing of AD/AV neurons, whereas cortical and subiculum inputs modulate the action of the MB inputs (Petrof and Sherman, 2009).

Input-Specific Modulation of Short-Term Plasticity by GSG1L

Inputs to AD/AV neurons undergo varying degrees of short-term plasticity upon repetitive stimulation (Petrof and Sherman, 2009). Given the high expression of GSG1L in AD/AV neurons, we wondered whether GSG1L is responsible for short-term plasticity. To address this, the extent of short-term plasticity in AD/AV neurons was compared between GSG1L KO and wild-type (WT) mice (Figures S1F–S1I). Sagittal sections were used to record from mammillothalamic (M-T) and subiculum-thalamic (S-T) synapses, whereas coronal sections were used to obtain corticothalamic (C-T) synapses (Figure 1I). We electrically stimulated the MB inputs (i.e., MTT) at 20 and 50 Hz while whole-cell recording from AD/AV neurons (Figures 1J–1L and S2A–S2C). The degree of synaptic depression in the M-T synapses was quantified by taking amplitude ratios of the first stimulus (S1) and following four stimuli

(S2–S5) responses. There was no statistical difference between GSG1L KO and WT control littermates (Figures 1J–1L and S2A–S2C). Similar results were obtained when inputs from the subiculum, the S-T synapses, were examined at 20 and 50 Hz (Figures 1M–1O and S2D–S2F). In contrast, stimulation of the C-T pathway of GSG1L KO, at both 20 and 50 Hz, resulted in enhanced synaptic facilitation, relative to WT control and heterozygous littermates (Figures 1P–1R and S2G–S2I). Similar findings were obtained when only AD synapses were examined, consistent with the close cellular pedigree of neurons in AD and AV (Shi et al., 2017) (Figures S2J–S2M).

Changes in the presynaptic glutamate release would affect both AMPARs and NMDA receptors (NMDARs). If short-term plasticity were mediated by a presynaptic mechanism, one would expect to find the effect of the genotype in both AMPAR-and NMDAR-mediated EPSCs. Therefore, to exclude the possibility of a presynaptic effect, we examined short-term plasticity of NMDAR-mediated EPSCs in the C-T synapses in response to 20 and 50 Hz stimulations (Figures S3A–S3E). We found no differences between GSG1L KO and control littermates, indicating that the effect is postsynaptic and AMPAR dependent. Input-specific stimulation of the C-T pathway unveiled the postsynaptic role of GSG1L, where its deletion is associated with enhanced synaptic short-term facilitation. Collectively, these results suggest that GSG1L input specifically regulates synaptic plasticity at AD/AV.

AMPAR Desensitization Occurs at C-T Synapses of AD/AV Neurons

If GSG1L regulates C-T synapses by altering the rate of recovery from desensitization of postsynaptic AMPARs, desensitization of AMPAR must be occurring during synaptic transmission. A simple way to test this is to examine sensitivity of evoked EPSCs to cyclothiazide (CTZ), a blocker of AMPAR desensitization. In GSG1L WT mice, whole-cell recordings from AD/AV neurons detected a significant increase in the degree of synaptic facilitation upon addition of 100 μM CTZ while stimulating the cortical inputs at 20 and 50 Hz in the presence picrotoxin, a blocker of γ-amino-butyric acid (GABA) A receptors (Figures S3F–S3J). Importantly, CTZ sensitivity in C-T synapses requires GSG1L, because it is absent from GSG1L KO (Figures S3F–S3J). This substantiates our hypothesis that GSG1L affects short-term plasticity in these synapses through a postsynaptic mechanism of slowing AMPAR recovery from desensitization.

GSG1L Modulates Basal Synaptic Transmission at C-T Synapses

Another predicted signature of synapses regulated by GSG1L is the reduction of amplitude of AMPAR-mediated responses (Figure 1A) (McGee et al., 2015). Thus, we next investigated whether GSG1L also regulates basal AMPAR-mediated synaptic transmission by recording AMPAR-mediated miniature EPSCs (mEPSCs) in AD/AV neurons from GSG1L KO and WT mice (Figures 2A–2D). We found no significant differences in the average amplitude or the frequency of AMPAR-mediated mEPSCs. However, upon careful inspection, we found that there was a subset of GSG1L KO neurons with enhanced amplitude of mEPSCs (Figure 2C). This is in agreement with GSG1L functionally regulating a subset of synapses, specifically those formed by C-T inputs (Figure 1).

To directly test whether GSG1L regulates basal synaptic transmission at C-T synapses, we recorded asynchronous quantal EPSCs (qEPSCs) evoked in the presence of strontium (4 mM $SrCl_2$) (Figures 2E–2L). Synaptic responses produced by isolated asynchronous quantal events represent postsynaptic AMPAR activity in the evoked pathway (Goda and Stevens, 1994). We found that the amplitude of asynchronous qEPSCs is enhanced in GSG1L KO animals relative to WT control (Figures 2E–2H). The frequency of qEPSCs was also higher in GSG1L KO C-T synapses, most likely because of an increase in apparent detection sensitivity caused by an increase in the amplitudes. In addition, consistent with GSG1L's role in modulating AMPAR gating kinetics (Schwenk et al., 2012; Shanks et al., 2012), the kinetics of C-T qEPSCs are accelerated in GSG1L KO. Although the difference in the rise time of qEPSCs was not significant ($p = 0.0900$), the decay time was significantly reduced in GSG1L KO (Figures 2I–2L).

Consistent with GSG1L having an input-specific function at AD/AV, there were no significant differences in the amplitude or frequency of asynchronous qEPSCs between GSG1L KO and WT in M-T synapses (Figures 2M–2O) or S-T synapses (Figures 2P–2R). The kinetics of qEPSCs in these two pathways were unaltered between GSG1L KO and WT (Figures S3K–S3P).

Functional Co-expression of GSG1L and Stargazin in AD/AV Neurons

Using the results of the Allen Brain Atlas as a reference, we inferred that stargazin is the dominant type I TARP expressed in AD/AV neurons (Figures S4A–S4E). A previous study has shown that stargazin outcompetes GSG1L in AMPAR gating modulation in *Xenopus* oocytes (Schwenk et al., 2012). To test the hypothesis that stargazin and GSG1L both modulate AMPARs at synapses in AD/AV neurons, we investigated the effect of deleting stargazin using a γ−2 KO mouse generated in our lab (Figures S4F–S4J).

In stargazer mice (i.e., spontaneously occurred γ−2 KO mice), there is complete loss of functional synaptic AMPARs in cerebellar granule cells (Hashimoto et al., 1999; Chen et al., 2000). In contrast, we found that in AD/AV neurons, there is residual AMPAR activity in γ−2 KO mice. Consistent with stargazin being a positive AMPAR regulator, both the amplitude and the frequency of AMPAR-mediated mEPSCs are lower in γ−2 KO relative to WT control (Figures 3A–3D). The residual mEPSCs indicate the existence of a subset of synapses with functional AMPARs. We predicted that these are C-T synapses do not have stargazin regulation but instead are controlled by GSG1L. We found no significant differences in the amplitude or the frequency of asynchronous qEPSCs between γ−2 KO and WT in C-T synapses (Figures 3E–3G). These results suggest that γ−2 plays a minimal role regulating C-T synapses in AD/AV neurons in the presence of GSG1L.

We predicted that stargazin is a dominant auxiliary subunit in M-T and S-T synapses, whereas GSG1L exclusively regulates C-T synapses. Consistent with this hypothesis, we found that removal of stargazin from AD/AV neurons unmasks the basal postsynaptic modulatory effect of GSG1L in GSG1L/γ−2 double-knockout (dKO) mice (Figures 3H–3K). Namely, both the amplitude and the frequency of mEPSCs are significantly increased in GSG1L/γ−2 dKO mice relative to GSG1L WT/γ−2 KO and GSG1L Het/γ−2 KO. Furthermore, consistent with the role of GSG1L in slowing AMPAR kinetics, both the rise

time and the decay time of mEPSCs are significantly reduced in GSG1L/γ−2 dKO relative to GSG1L WT/γ−2 KO neurons (Figures 3L–3N). Altogether, these findings indicate that under basal conditions, stargazin outcompetes GSG1L in modulating AMPARs in M-T and S-T synapses. The action of GSG1L on basal synaptic transmission is fully unmasked in the GSG1L/γ−2 dKO mouse.

Increased Hyperexcitability and Enhanced Seizure Susceptibility in GSG1L KO

Having established the synaptic function of GSG1L, we next investigated whether the loss of GSG1L would result in circuit-level changes in excitability. To test this, we recorded spontaneous action potential firing of AD/AV neurons in current-clamp mode with no current injection. We found that 60% of GSG1L KO AD/AV neurons spiked during a 3-min recording period, whereas only 15% spiked in WT neurons (Figures 4A–4C). There was no change in intrinsic excitability of neurons in GSG1L KO, because no differences were observed in the resting membrane potential, rheobase, and neuronal firing rate between GSG1L KO and WT control (Figures S5A–S5D). However, the input resistance is significantly reduced in GSG1L KO mice (Figure S5E), which is consistent with increased synaptic activity, although it may not be the sole cause of the effect. In addition, we found that spontaneous excitatory synaptic transmission is significantly enhanced in GSG1L KO mice (Figures 4D–4F), as well as in GSG1L/γ−2 dKO mice (Figures S5F–S5I). Both the amplitude and the frequency of AMPAR-mediated spontaneous EPSCs (sEPSCs) are increased in GSG1L KO neurons. Altogether, neurons in AD/AV neurons of GSG1L KO mice are hyperactive overall.

Next, we aimed to evaluate the effect of the loss of GSG1L at the organism level. Initial basic behavioral phenotyping of GSG1L KO mice revealed no differences in grip strength, rotarod performance, elevated zero maze, and gait parameters (Figures S5J–S5M). However, we found that GSG1L KO mice show deficits in a novel object recognition (NOR) task (Figure S5N), similar to the findings of previous reports using GSG1L KO rats (Gu et al., 2016). These results are consistent with the known role of AT in learning and memory (Parker and Gaffan, 1997), but a more drastic behavioral phenotype was revealed when the animals were challenged with seizure, a condition in which AT plays a critical role (Mirski and Ferrendelli, 1984; Bittencourt et al., 2010).

We found that GSG1L KO mice exhibit enhanced susceptibility to kainate-induced seizures (Figures 4G–4J). The seizure severity was determined on a scale of 0–7, a rating system with increasing severity in an ascending scale and with a score 7 denoting death (Morrison et al., 1996). At a lower-dose injection (15 mg/kg intraperitoneal [i.p.]) of kainate, GSG1L KO mice had a significantly higher seizure severity score than WT controls. Furthermore, 23% (3 of 13 mice) of GSG1L KO mice, and no GSG1L WT mice, died within 2 h after kainate administration. At a higher-dose injection (25 mg/kg i.p.) of kainate, 75% of GSG1L KO mice died within 2 h postinjection and only 25% of WT mice. These results highlight the *in vivo* importance of GSG1L in protecting against kainate-induced neurotoxicity and pathological hyperexcitability. Consistent with GSG1L being a negative regulator of AMPAR function, GSG1L KO mice have enhanced excitatory neurotransmission and susceptibility to seizures, along with increased spontaneous firing of AD/AV neurons.

DISCUSSION

AD/AV, where GSG1L is abundantly expressed, is at the core of the extended hippocampal-diencephalic network with crucial roles in memory (Aggleton and Brown, 1999); thus, AD/AV damage is associated with anterograde amnesia (Ghika-Schmid and Bogousslavsky, 2000; Gold and Squire, 2006). AD/AV contains neurons that sense head direction during spatial navigation (Clark and Taube, 2012) and have been implicated in seizure initiation and/or propagation (Mirski and Ferrendelli, 1984; Kerrigan et al., 2004). In contrast to the extensively studied lateral geniculate nucleus (LGN), molecular and functional characterization of the synapses of AD/AV is largely lacking.

We found that GSG1L and stargazin are functionally co-expressed in AD/AV. Among the synapses in AD/AV neurons formed by three distinct input projections, C-T synapses are controlled by GSG1L, but not by stargazin (Figures 1, 2, and 3). In C-T synapses, GSG1L reduces the amplitude and slows the kinetics of AMPAR-mediated qEPSCs and suppresses short-term facilitation by slowing recovery from desensitization. GSG1L promotes surface expression of AMPARs in HEK cells and hippocampal neurons (Shanks et al., 2012; Gu et al., 2016), and such a mechanism may partially contribute to the properties of C-T synapses. However, we suggest that the effect of GSG1L on gating modulation plays a dominant role in regulating short-term plasticity given the CTZ sensitivity of these synapses in WT, but not in GSG1L KO (Figures S3F–S3J).

In contrast to GSG1L, stargazin plays a major role in M-T or S-T synapses (Figure 4K). The mechanism that restricts the functions of GSG1L and stargazin to specific afferent synapses remains to be determined. We speculate that presynaptic terminals may provide some *trans*-synaptic molecular cues, considering that GSG1L lacks a PDZ (PSD-95, dlg, ZO-1) domain binding motif in the cytoplasmic C terminus as it would normally facilitate synaptic anchoring.

In *Xenopus* oocytes, stargazin outcompetes GSG1L in AMPAR modulation (Schwenk et al., 2012), which agrees with GSG1L and stargazin sharing identical binding sites on AMPARs (Twomey et al., 2016, 2017b). In AD/AV, we also found that under basal conditions, stargazin outcompetes GSG1L, functionally, in most synapses (Figures 3H–3N). The effect of GSG1L is unmasked in GSG1L/γ−2 dKO mice. These observations also indicate that in AD/AV, the C-T synapses are the smaller population compared with the combined sets of M-T and S-T synapses.

Similar to GSG1L, CKAMP44 slows recovery from desensitization, modulates short-term plasticity, and is expressed in AD/AV (Figure S4E) (von Engelhardt et al., 2010; Chen et al., 2018). We found that M-T synapses in AD/AV undergo pronounced STD (Figures 1J–1L and S2A–S2C), which is highly sensitive to CTZ (data not shown). Given that GSG1L does not modulate AMPARs at M-T synapses, we speculate that CKAMP44 could be postsynaptically functional in these synapses, which has yet to be investigated. Again, input-specific functional expression of an AMPAR auxiliary subunit in the thalamus may extend to the case of CKAMP44.

Consistent with GSG1L being a negative regulator of AMPAR function, deletion of GSG1L results in hyperexcitability in the AT (Figure 4), with its impact observed in the downstream cortical neurons (data not shown). Moreover, GSG1L KO mice have enhanced susceptibility to kainate-induced seizures. We suggest that disturbed excitation/inhibition (E/I) balance in GSG1L KO is associated with seizure states (Bateup et al., 2013; Paz and Huguenard, 2015; Staley, 2015). Circumstantial evidence suggests GSG1L may serve a neuroprotective role against hyperexcitability and ischemia (Keum and Marchuk, 2009; Du et al., 2015). GSG1L was identified as one of the candidate genes at the locus that determines the extent of infarct volume in mouse models of focal cerebral ischemia (Keum and Marchuk, 2009). Furthermore, a suggestive single-nucleotide polymorphism in GSG1L was found to be associated with infarct volume upon ischemic stroke in mice and human patients (Du et al., 2015). However, these are correlative studies, and further investigation is needed to the test the direct link between GSG1L and ischemia.

Previous investigations on the synaptic phenotypes of GSG1L KO rats in CA1 and DG (dentate gyrus) neurons (Gu et al., 2016; Mao et al., 2017) were both conducted at time points when the expression of the lacZ reporter for GSG1L promoter activity is low (Figures S1C and S1D). Specifically, GSG1L KO rat acute slices at postnatal day (P) 13–P19 were used. Although GSG1L protein is detectable in a subset of dendritic spines in older neurons (Schwenk et al., 2012; Shanks et al., 2012; Willems et al., 2020), the overall expression of GSG1L may be low in the hippocampus compared with the AT at young age (i.e., P13–P19). In agreement with such a hypothesis, a previous study on GSG1L KO rat reported a substantial contribution of another auxiliary subunit, CNIH2, superimposed on the functional effect of GSG1L (Gu et al., 2016). However, because the lacZ reporter is an indirect indicator of GSG1L protein expression, future studies using more direct methods are necessary to determine whether its expression is low in young hippocampus.

AMPAR desensitization is critical for normal brain function (Christie et al., 2010). CKAMP44 regulates AMPAR desensitization and contributes to the underlying mechanism of STD in retinogeniculate synapses (Chen et al., 2018, 2000; Kielland and Heggelund, 2002; Budisantoso et al., 2012). The glomerular structure of the retinogeniculate synapse has large terminals and closely spaced release sites (Rafols and Valverde, 1973). The unique overall geometry prevents fast removal of glutamate and allows spillover, resulting in AMPAR desensitization (Budisantoso et al., 2012). However, the corticogeniculate synapses have single distant synaptic contacts (Erişir et al., 1997; Narushima et al., 2016) with low release probability (Granseth et al., 2002). In these synapses, AMPAR desensitization is predicted to not contribute to short-term plasticity, such as observed in the ventrobasal nucleus (Sun and Beierlein, 2011). CKAMP44 plays no role in short-term plasticity at corticogeniculate synapses in the LGN (Chen et al., 2018). In contrast, we found that AMPAR desensitization substantially contributes to short-term plasticity at C-T synapses in AD/AV. GSG1L is highly expressed in AD/AV (Figures 1 and S1), but not in the LGN or ventrobasal nuclei of the thalamus (Lein et al., 2007). Hence, it is uniquely positioned to regulate short-term plasticity in C-T synapses in AD/AV, despite its predicted ultrastructure and low release probability.

STAR★METHODS

RESOURCE AVAILABILITY

Lead contact—Further information and requests for resources and reagents should be directed to the Lead Contact, Terunaga Nakagawa (terunaga.nakagawa@vanderbilt.edu).

Materials availability—Requests that are related to mouse lines, should be directed to the lead contact.

Data and code availability—The data generated during this study are available from the lead contact upon reasonable request.

EXPERIMENTAL MODEL AND SUBJECT DETAILS

All animal procedures were approved by the Vanderbilt University Animal Care and Use Committee and were in agreement with the NIH and Vanderbilt University guidelines for the care and use of laboratory animals. Mature mice and rats were housed with same-sex littermates and maintained on a 12hr light/dark cycle under controlled temperature and humidity. Food and water were provided *ad libitum*.

A GSG1L knockout (KO) transgenic mouse line was generated by targeting exon 4 of GSG1L gene in 129/SvEvTac embryonic stem (ES) cells. Two independent clones were shown by Southern blot analysis and PCR to have undergone proper homologous recombination and germline transmission was confirmed from chimeras derived from clone 2H2. To remove the pGK-neo cassette, the 3-loxP mouse was crossed with FlpE line (Rodríguez et al., 2000) that ubiquitously expresses Flp recombinase, generating a 2-loxP animal. Finally, by crossing with EIIa-cre mice (JAX: Stock 003724, which was backcrossed with C57BL6/J over 10 generations) that expresses cre-recombinase in the one cell zygote, we obtained the 1-loxP heterozygotes. All strains were backcrossed with C57BL6/J mice for 8 generations. All KO animals were viable with no overt issues with breeding and/or development.

The γ−2 KO mouse was generated as follows: A 20 bp sequence (TGAAACCAGCAAGAAGAACG, boxed in Figure S4) followed by AGG as proto-spacer adjacent motif (PAM), was selected within exon 1 of the CACNG2 (encoding γ−2) mouse gene to create a target-specific guide RNA molecule. The sequence flanked by *BbsI* sites was ligated in pX330, a vector expressing the guide RNA under a strong U6 promoter and cas9 under a hybrid chicken beta-actin (Cbh) promoter. The vector was injected alongside a 195 base repair single stranded oligonucleotide into 314 mouse embryos. The repair oligo contained 90 bp homology arms, a codon substituting lysine residue 53 to a stop codon, a unique *AgeI* restriction site, and a few additional third base mutations to prevent targeting of cas9 to the repaired DNA (Figure S4). Out of 314 embryos injected, 267 were transferred to 11 pseudo-pregnant females to generate 16 pups. At weaning, genotyping was done by amplifying a 926 bp fragment followed by sequencing. Out of 15 pups (one died prior to weaning), only one animal (female #12) carried the designed mutation. After several backcrossing to C57BL6/J mice to eliminate any possible off target events, heterozygote mice were crossed to generate homozygous KO animals.

A transgenic GSG1L KO rat line in the background of SD strain was among the mutants generated through transposon-based mutagenesis by Kent Hamra at UT Southwestern (Izsvák et al., 2010). The mutant rat line was purchased and maintained in house.

For each experiment, both male and female animals were used. Each cohort contained roughly equal number of each sex. For short-term plasticity experiments comparing the three pathways, GSG1L KO and WT mice P21-P33 were used. For short-term plasticity experiments of AD only, AD/AV combined, NMDAR-dependent, and CTZ recordings were done at P15-P30. For mEPSCs, sEPSCs, qEPSCs and current clamp recordings of GSG1L KO and WT mice at P15-P30 were used. For mEPSCs and sEPSCs of γ−2 KO and WT (and GSG1L/γ−2 dKO) mice at P15-P22 were used. For behavioral experiments, GSG1L KO and WT mice at 9–10 month old were used. LacZ staining of GSG1L KO rat and WT control littermates was done as indicated in the figures: P14, P21, P60, and P180.

Genotyping by PCR

PCR amplification was conducted with the following primers:

GSG1L KO mice: GSG1L left: aaacagacaacatggccctcagactc; GSG1L right: gacttgtcccatctctaggatacctccc.

GSG1L KO rats: Gsg1L left: acgttgtagtgaccccaagc; GSG1L right: tgcacgcatactacaatga; SFB2: tcatcaaggaaaccctggac

γ−2 KO mice: CAC9: atggtgttgagaattcggctgtacc; CAC10: aaccctaaggactccaaagcatcc

METHOD DETAILS

Electrophysiology in acute slices—For all electrophysiology experiments that were done in the AT, mice of both sexes aged were used. Using the stria medullaris (sm) and the hippocampus as anatomical landmarks, we unambiguously identified AD/AV in 300 μm-thick coronal sections. For short-term plasticity experiments, the C-T synapse was isolated in a coronal slice configuration and the cortical inputs were stimulated outside of AD/AV (as illustrated in Figures 1H and 1I). M-T synapses were isolated in 300 μm-thick sagittal brain sections. The prominent MTT and the hippocampus were used as anatomical landmarks to identify the AD/AV. To stimulate this synapse, the stimulating electrode was placed directly on the MTT. The S-T synapse was isolated in 300 μm-thick sagittal brain sections. The MTT and the hippocampus were used as landmarks to isolate the AD/AV and the electric stimulator was placed on the subiculum inputs directly below the hippocampus.

Mice were decapitated and the brains were rapidly removed and placed in ice-cold *N*-methyl-D-glucamine (NMDG) cutting solution containing 92 mM NMDG, 2.5 mM KCl, 30 mM $NaHCO_3$, 1.25 mM NaH_2PO_4, 11 mM Glucose, 0.5 mM $CaCl_2$, 10 mM $MgCl_2$, 20 mM HEPES, 2 mM thiourea, 5 mM Na-ascorbate, 3 mM Na-pyruvate, with pH adjusted to 7.4 with HCl. Acute 300 μm-thick slices were prepared using a vibratome (Leica VT 1200). Slices were then left to recover for 1 hr in artificial cerebro-spinal fluid (aCSF) solution containing 119 mM NaCl, 2.5 mM KCl, 26 mM $NaHCO_3$, 1 mM NaH_2PO_4, 11 mM Glucose, 1 mM $MgCl_2$, 2 mM $CaCl_2$, at pH 7.4 and 310 mOsm, saturated with 95%O_2/5% CO_2.

For AMPAR-mediated mEPSCs recordings, the aCSF was supplemented with tetrotodoxin (TTX, 0.5 μM) in order to suppress spontaneous excitation. To specifically isolate AMPAR-mediated mEPSCs at a holding potential of −70mV, GABA-A receptor activity was blocked with 100 μM picrotoxin (Tocris). For AMPAR-mediated sEPSCs recordings, the aCSF was supplemented with 100 μM picrotoxin to isolate the AMPAR component at −70 mV. Pipettes were filled with the internal solution containing 115 mM Cs methanesulfonate, 20 mM CsCl, 10 mM HEPES, 2.5 mM $MgCl_2$, 4 mM Na_2ATP, 0.4 mM Na_3GTP, 10 mM Na phosphocreatine, and 0.6 mM EGTA. The osmolarity was adjusted to 295 mOsm and the pH was adjusted to 7.25 with CsOH. The patches were formed with borosilicate glass pipettes (O.D. 1.5mm, I.D. 0.86mm, Sutter) (3–5 MΩ tip resistance). Recordings were made using Multiclamp 700B Amplifier (Axon Instruments) operated by pCLAMP10 software, low-pass filtered at 10 kHz and digitized at 20 kHz using Digidata1440A (Axon Instruments). Obtained mEPSCs and sEPSCs events were detected and analyzed with NeuroMatic event detection software (IGOR-pro, Wavemetrics) and correct event detection was confirmed by manual visual inspection, while errors were corrected by manual inspection of the traces. All the recordings and analysis were done in a blind manner, with the experimenter blind to the genotype during data acquisition and analysis. Significance was determined with Mann-Whitney U-test or a two-way analysis of variance (Two-Way ANOVA) with Sidak's multiple comparison post hoc test when applicable.

To evoke asynchronous quantal EPSCs (qEPSCs), Ca^{2+} was replaced with Sr^{2+} (4 mM $SrCl_2$). In order to avoid the multiquantal events, we only analyzed the qEPSCs that occurred > 10 ms following the stimulation with the total sweep duration of 360 ms. Obtained qEPSC events were detected and analyzed with NeuroMatic event detection software (an extension to the IGOR-pro, Wavemetrics) and correct event detection was confirmed, while errors were corrected by manual inspection of the traces. The kinetic analysis of qEPSCs and mEPSCs were also done using NeuroMatic and IGOR-pro. From each corresponding cell, all isolated events with flat baseline were used for analysis. Typically, from each cell 15–30 representative events with monotonic rise and distinct decay were selected and averaged. The decay time of averaged qEPSCs was determined by fitting to double exponential function. The weighted decay time constant was further calculated as sum of slow and fast time constants and weighted by fractional amplitudes (Hawken et al., 2017).

For short-term plasticity experiments, whole-cell recordings AD/AV neurons were achieved in response to electrical stimulation of MTT, subiculum, or the cortical inputs at a holding potential of −70 mV. For M-T recordings, 300 μm-thick acute sagittal slices with AD/AV and visible MTT were obtained. The MTT was electrically stimulated, and current changes were recorded in response to 5-pulse stimulation at 20 Hz and 50 Hz. For S-T recordings, 300 μm-thick acute sagittal slices with AD/AV were obtained. Similarly, the subiculum inputs (as depicted in Figure 2) were stimulated at 20 Hz and 50 Hz. For C-T recordings, 300 μm-thick acute coronal slices with AD/AV were obtained and the cortical inputs (as depicted in Figure 2) were electrically stimulated at 20 Hz and 50 Hz. Slices were perfused with aCSF supplemented with 100 μM picrotoxin. To isolate the effect of CTZ on short-term plasticity, we bath applied aCSF supplemented with 100 μM CTZ (Tocris). NMDAR currents were recorded as aforementioned, but at a holding potential of +40 mV and in the

presence of 10 μM NBQX and 100 μM picrotoxin. Statistical significance was assessed using a two-way analysis of variance (Two-Way ANOVA) with Sidak's multiple comparison post hoc test.

Intrinsic excitability properties were analyzed in current clamp recording mode. The recordings were done using potassium-based internal solution containing: 115mM K methanesulfonate, 20 mM KCl, 10 mM HEPES, 2.5 mM $MgCl_2$, 4 mM Na_2ATP, 0.4 mM Na_3GTP, 10 mM Na phosphocreatine, 0.6 mM EGTA. The osmolarity was adjusted to 295 mOsm and the pH was adjusted to pH 7.25 with KOH. In order to measure the intrinsic excitability properties, the neurons were held at −70 mV and current was injected in 10 pA increments (from −20 to 160 pA) for 200 ms. The rheobase was determined as a minimal current injection required to elicit an action potential firing. The firing rate was determined as the number of action potentials fired at 150 pA injection. The input resistance was determined by calculating the slope of current-voltage plot (−20 to 20 pA). The firing frequency of spiking GSG1L KO neurons was determined, by calculating the frequency of fired action potentials during a 50 msec recording period.

Fast glutamate application from outside out patches—TetON HEK cells were plated on a coverglass coated with poly-D-lysine (37.5 μg/ml in H_2O) for 15 min. Excess coating material was removed by washing in D-PBS three times. Cells were plated and incubated on a coverglass until they were adherent (typically within 12 hr) and transfected with a plasmid (DualpTREt-GluA2i(Q)+GSG1L) that DOX dependently express GluA2flip(Q) and GSG1L. After transfection, 30 μM NBQX and 5 μg/ml doxycycline (DOX) were added. Cells were used for recording 24–36 hr after induction. Ligand (1mM glutamate) was applied via theta tubing glass capillary mounted on a piezo actuator (P-830.30, Physik Instrumente) controlled by an LVPZT amplifier (E-505, Physik Instrumente), DAQ device (NI USB-6221, National Instruments), and LabView software (National Instruments). Recording was done using a single channel of a Multiclamp700B Amplifier (Axon Instruments) operated by pCLAMP10 software. Signals were digitized using Digidata1440A (Axon Instruments) at a sampling rate of 50 kHz and low pass filtered at 2kHz. Borosilicate glass capillaries (O.D. 1.5 mm, I.D. 0.86 mm, Sutter) were pulled to manufacture electrodes with pipette resistances of 4–5 MΩ. Internal solution was (in mM) 110 NaCl, 10 NaF, 5 EGTA, 0.5 $CaCl_2$, 1 $MgCl_2$, 10 Na_2ATP, 5 HEPES, adjusted to pH 7.3 with CsOH and 295 mOsm. External solution was (in mM) 145 NaCl, 2.5 KCl, 1.8 $CaCl_2$, 1 $MgCl_2$, 5 HEPES, 10 glucose, adjusted to pH 7.3 with NaOH and 301 mOsm. Standard solution without ligand was the external solution. The ligand solution contained 1mM glutamate in external solution, supplemented with 2 mM glucose and 3 mM NaCl to facilitate the visualization of the interface of the two solutions and recording liquid junction potential after breaking the patch. A protocol for four 1ms glutamate pulses at 20Hz was programmed using LabView. The 20%–80% rise time of liquid junction potential, measured after breaking the patch, was ~300 μs.

BEHAVIORAL EXPERIMENTS

Seizure behavior—To investigate seizure susceptibility behavior, GSG1L KO and WT littermates of both sexes (9–10 month old) were administered an intraperitoneal (i.p.)

injection of kainic acid monohydrate (Sigma) dissolved in 0.9% saline solution at 15 mg/kg or 25 mg/kg body weight. Seizure susceptibility was determined immediately following the kainate injections. Seizure activity was video recorded for 2 hr and scored for severity using a previously described seizure severity scale in a blind manner, with the experimenter blind to the genotype during scoring (Morrison et al., 1996; Wu et al., 2005; Bateup et al., 2013). Seizure severity was assessed at a five-minute interval.

The severity of seizures was assigned based on the following chart:

0, no abnormality;

1- immobility, cessation of normal behavior;

2- rigid posture with extended tail or forelimbs;

3- repetitive behaviors including head nodding, head bobbing, twitching, or scratching;

4- Forelimb clonus with partial or intermittent rearing;

5- continuous forelimb clonus/rearing or repeated rearing and falling;

6- loss of posture, generalized tonic-clonic whole body convulsions or hyperactivity/jumping behavior;

7- mortality.

Novel object recognition task—GSG1L KO and WT littermates of both sexes (9–10 month old) were habituated for 10 min in an empty novel object recognition arena (40 × 64 × 33 cm^3) on day 1. The following day, the mice were placed in the novel object recognition arena that contained two identical objects and were allowed to explore the space for 10 min. Following the habituation phase, mice were placed back into their homecage for 1 hr. During probe phase, one of the familiar (previously exposed) objects was replaced with a novel object. The exploration behavior was recorded for 10 min. Time spent exploring familiar and novel objects was scored blindly and the recognition index was identified as (time exploring novel object)- (time exploring familiar object) / total time exploring both objects.

Rotarod—Motor coordination and balance were measured by placing the mice on an accelerating rotating rod (Ugo Basile model 7650; Stoelting Co., Wood Dale, IL, USA). The initial rotations per minute (rpm) were set at 4 rpm, which gradually increased to 40 rpm. The performance of each animal was recorded over the course of 300 s. The time taken for a mouse to fall off the rod was recorded by an observer blinded to the mouse genotype. The test was conducted over the course of three days with three independent trials per day.

Elevated Zero Maze—Anxiety was measured using elevated zero maze (San Diego Instruments, CA). The device is an elevated ring-shaped platform with four equal chambers (two open arms and two closed arms). Light levels in the closed arms were at approximately 100 lux and 200 lux in open arms. Mice were placed in the center of an open arm and allowed to explore the maze for 5 min. The activity was video-recorded and analyzed using ANY-maze software (Stoelting, Wood Dale, Illinois, USA).

Grip strength—Grip strength was measured using a Grip Strength Test Apparatus (San Diego Instruments, CA). The grip strength was measured by a digital gauge over 7 independent trials. The average grip strength was calculated as an average of 7 trials (in Newtons).

Histology—GSG1L KO (P14, P21, P60, P180) rat brains with corresponding WT rat animals were anesthetized with sodium pentobarbital (Nembutal). Each animal was then perfused with normal rat Ringer solution (pH 7.4) for 2 min to ensure complete perfusion, followed by 4% paraformaldehyde in 0.1M phosphate (pH 7.4) buffer for 4 min. Obtained brains were further fixed for 15 min. Fixed brains were subsequently sectioned to generate 300 μm-thick coronal sections using a vibratome (Leica VT 1200). The sections were then permeabilized with 0.01% Sodium deoxycholate and 0.02% Triton X-100 in PBS buffer for 2 hr. Following permeabilization, 300 μm-thick coronal sections were incubated with X-gal staining solution containing: 5 mM $K_3[Fe(CN)_6]$, 5 mM $K_4[Fe(CN)_6]$, 2 mM $MgCl_2$, 0.02% Triton X-100, and 0.1% X-gal in PBS buffer at 37°C for 8 hr in the dark. Stained brains were imaged (MULTIZOOM AZ100M, Nikon microscope) following day (1 day post staining).

Confirming the absence of targeted proteins in the KO animals—Immunoprecipitation of protein complexes were performed as previously described (Nakagawa et al., 2005). Briefly, mouse (or rat) brains were homogenized in 20 mM HEPES pH 7.4, 320 mM sucrose, 5 mM EDTA, 5 mM EGTA, 30 μM NBQX supplemented with protease inhibitors 1 mM PMSF, 10 μg/ml aprotinin, 10 μg/ml leupeptin, 1 μg/ml pepstatin, and 500 μM benzamidine. Brain homogenates were spun down at 3000 g for 15 min and the obtained supernatant was further spun at 38,400 g for 15 min resulting in a membrane pellet. The membrane pellet was resuspended in a buffer containing 20 mM HEPES pH 7.4, 1 M KI, 5 mM EDTA, 5 mM EGTA, and 30 μM NBQX. To wash off the KI, membranes were washed with wash buffer containing 20 mM HEPES pH 7.4, 5 mM EDTA, 5 mM EGTA, and 30 μM NBQX. The final membrane pellet was solubilized in a resuspension buffer containing 20 mM HEPES pH 7.4, 100 mM NaCl, 5 mM EDTA, 5 mM EGTA, 1% CHAPS, 30 μM NBQX and the protease inhibitors for two hours at 4°C. To validate GSG1L 3-loxP KO, GSG1L was immunoprecipitated with previously described anti-GSG1L Ct2 antibody (2mg/ml) and eluted with the epitope peptide CKVFEQGYREEPTFIDPEAIKYFR (Shanks et al., 2012). To validate GSG1L 1-loxP KO, GSG1L was immunoprecipitated with anti-GSG1L Ct1 antibody (2mg/ml) and eluted with the epitope peptide CRSSAHEAAELNRQCWVLGHWV (Shanks et al., 2012). Immunoprecipitated GSG1L from the brain lysates of 3-loxP KO and 1-loxP KO GSG1L was then probed in western blots with anti-GSG1L Ct1 antibody and Ct2 antibody, respectively. Of note, long and short isoforms of GSG1L transcripts are listed in the mouse genome database. The short isoform is predicted to lack the Ct2 epitope, and thus we were only able to confirm the KO of 43kDa long isoform of GSG1L. The short isoform lacks the TM4, which is essential for binding AMPAR from the cryo-EM structure (Twomey et al., 2017b), and unlikely to have a role in regulating AMPAR. The folding of TM1-TM4 is highly conserved among the tetraspanins and therefore loss of TM4 is likely to cause a substantial misfolding in the short isoform. Specifically, if the short isoform exists, it would have an extracellular C-terminal, whose

topology is completely different from the long isoform with a cytoplasmic C-terminal. Moreover, our targeting design does not permit efficient transcription of the shorter isoform given that exon 4, upstream of the putative splice site, is targeted. Collectively, we suggest that the short isoform is unlikely to exist and only the long isoform is relevant in the current study. We also note that the observed differences in the non-specific band patterns in Figure S1I is a consequence of using different polyclonal antibodies for detection. Note that the band immediately below GSG1L in 1loxp KO blot is due to nonspecific binding (Figure S1I). For validating γ−2 KO, AMPAR complexes were pulled down with anti-GluA2 antibody (EGYNVYGIESVKI). Immunoprecipitated stargazin was probed with anti-stargazin antibody (Millipore, AB9876).

QUANTIFICATION AND STATISTICAL ANALYSIS

All statistical analyses were performed with Graphpad Prism. Data in the figures are represented as mean ± SEM. The information on statistical tests used, sample sizes (n) and animal subjects (N) are present in figure legends. Statistical significance for averaged data from multiple experiments was determined using Mann-Whitney U test or Two-Way Analysis of Variance (ANOVA) followed by Post hoc analysis. Error bars in all figures represent standard error of the mean. The cumulative probability difference was determined using Kolmogorov-Smirnov test.

Supplementary Material

Refer to Web version on PubMed Central for supplementary material.

ACKNOWLEDGMENTS

Behavioral testing was performed at the Vanderbilt Mouse Neurobehavioral Laboratory, which is supported by the EKS NICHD of the NIH under award U54HD083211. We acknowledge the use of Vanderbilt Cell Imaging Shared Resource and Vanderbilt Transgenic Core (the current Vanderbilt Genome Editing Resource). We thank Elena Zaika for technical support. We also thank Kent Hamra for providing GSG1L KO rat. We thank Bob Matthews and John Allison for discussion and technical support. We also thank Jake Watson, Alexandra Pinggera, Akihiro Harada, Brian Shonesy, Fiona Harrison, Roger Col-bran, Sachin Patel, and Ege Kavalali for discussion. This work was funded by Vanderbilt University (to T.N.), NARSAD Independent Investigator Grant (to T.N.), and NIH grants R01HD061543 (to T.N.) and R01NS085215 (to K.F.).

REFERENCES

Aggleton JP, and Brown MW (1999). Episodic memory, amnesia, and the hippocampal-anterior thalamic axis. Behav. Brain Sci 22, 425–444, discussion 444–489. [PubMed: 11301518]

Bateup HS, Johnson CA, Denefrio CL, Saulnier JL, Kornacker K, and Sabatini BL (2013). Excitatory/inhibitory synaptic imbalance leads to hippocampal hyperexcitability in mouse models of tuberous sclerosis. Neuron 78, 510–522. [PubMed: 23664616]

Bittencourt S, Dubiela FP, Queiroz C, Covolan L, Andrade D, Lozano A, Mello LE, and Hamani C (2010). Microinjection of GABAergic agents into the anterior nucleus of the thalamus modulates pilocarpine-induced seizures and status epilepticus. Seizure 19, 242–246. [PubMed: 20347349]

Bowie D (2008). Ionotropic glutamate receptors & CNS disorders. CNS Neurol. Disord. Drug Targets 7, 129–143. [PubMed: 18537642]

Budisantoso T, Matsui K, Kamasawa N, Fukazawa Y, and Shigemoto R (2012). Mechanisms underlying signal filtering at a multisynapse contact. J. Neurosci 32, 2357–2376. [PubMed: 22396411]

Cais O, Herguedas B, Krol K, Cull-Candy SG, Farrant M, and Greger IH (2014). Mapping the interaction sites between AMPA receptors and TARPs reveals a role for the receptor N-terminal domain in channel gating. Cell Rep. 9, 728–740. [PubMed: 25373908]

Chen L, Chetkovich DM, Petralia RS, Sweeney NT, Kawasaki Y, Wenthold RJ, Bredt DS, and Nicoll RA (2000). Stargazin regulates synaptic targeting of AMPA receptors by two distinct mechanisms. Nature 408, 936–943. [PubMed: 11140673]

Chen X, Aslam M, Gollisch T, Allen K, and von Engelhardt J (2018). CKAMP44 modulates integration of visual inputs in the lateral geniculate nucleus. Nat. Commun 9, 261. [PubMed: 29343769]

Christie LA, Russell TA, Xu J, Wood L, Shepherd GM, and Contractor A (2010). AMPA receptor desensitization mutation results in severe developmental phenotypes and early postnatal lethality. Proc. Natl. Acad. Sci. USA 107, 9412–9417. [PubMed: 20439731]

Clark BJ, and Taube JS (2012). Vestibular and attractor network basis of the head direction cell signal in subcortical circuits. Front. Neural Circuits 6, 7. [PubMed: 22454618]

Du R, Zhou J, Lorenzano S, Liu W, Charoenvimolphan N, Qian B, Xu J, Wang J, Zhang X, Wang X, et al. (2015). Integrative Mouse and Human Studies Implicate ANGPT1 and ZBTB7C as Susceptibility Genes to Ischemic Injury. Stroke 46, 3514–3522. [PubMed: 26542693]

Erişir A, Van Horn SC, Bickford ME, and Sherman SM (1997). Immunocytochemistry and distribution of parabrachial terminals in the lateral geniculate nucleus of the cat: a comparison with corticogeniculate terminals. J. Comp. Neurol 377, 535–549. [PubMed: 9007191]

Everett KV, Chioza B, Aicardi J, Aschauer H, Brouwer O, Callenbach P, Covanis A, Dulac O, Eeg-Olofsson O, Feucht M, et al. (2007). Linkage and association analysis of CACNG3 in childhood absence epilepsy. Eur. J. Hum. Genet 15, 463–472. [PubMed: 17264864]

Floor K, Barøy T, Misceo D, Kanavin OJ, Fannemel M, and Frengen E (2012). A 1 Mb *de novo* deletion within 11q13.1q13.2 in a boy with mild intellectual disability and minor dysmorphic features. Eur. J. Med. Genet 55, 695–699.

Ghika-Schmid F, and Bogousslavsky J (2000). The acute behavioral syndrome of anterior thalamic infarction: a prospective study of 12 cases. Ann. Neurol 48, 220–227. [PubMed: 10939573]

Goda Y, and Stevens CF (1994). Two components of transmitter release at a central synapse. Proc. Natl. Acad. Sci. USA 91, 12942–12946. [PubMed: 7809151]

Gold JJ, and Squire LR (2006). The anatomy of amnesia: neurohistological analysis of three new cases. Learn. Mem 13, 699–710. [PubMed: 17101872]

Granseth B, Ahlstrand E, and Lindström S (2002). Paired pulse facilitation of corticogeniculate EPSCs in the dorsal lateral geniculate nucleus of the rat investigated *in vitro*. J. Physiol 544, 477–486. [PubMed: 12381820]

Greger IH, Watson JF, and Cull-Candy SG (2017). Structural and Functional Architecture of AMPA-Type Glutamate Receptors and Their Auxiliary Proteins. Neuron 94, 713–730. [PubMed: 28521126]

Gu X, Mao X, Lussier MP, Hutchison MA, Zhou L, Hamra FK, Roche KW, and Lu W (2016). GSG1L suppresses AMPA receptor-mediated synaptic transmission and uniquely modulates AMPA receptor kinetics in hippocampal neurons. Nat. Commun 7, 10873. [PubMed: 26932439]

Hamani C, Ewerton FI, Bonilha SM, Ballester G, Mello LE, and Lozano AM (2004). Bilateral anterior thalamic nucleus lesions and high-frequency stimulation are protective against pilocarpine-induced seizures and status epilepticus. Neurosurgery 54, 191–195, discussion 195–197. [PubMed: 14683557]

Hamdan FF, Gauthier J, Araki Y, Lin DT, Yoshizawa Y, Higashi K, Park AR, Spiegelman D, Dobrzeniecka S, Piton A, et al.; S2D Group (2011). Excess of *de novo* deleterious mutations in genes associated with glu tamatergic systems in nonsyndromic intellectual disability. Am. J. Hum. Genet 88, 306–316. [PubMed: 21376300]

Hashimoto K, Fukaya M, Qiao X, Sakimura K, Watanabe M, and Kano M (1999). Impairment of AMPA receptor function in cerebellar granule cells of ataxic mutant mouse stargazer. J. Neurosci 19, 6027–6036. [PubMed: 10407040]

Hawken NM, Zaika EI, and Nakagawa T (2017). Engineering defined membrane-embedded elements of AMPA receptor induces opposing gating modulation by cornichon 3 and stargazin. J. Physiol 595, 6517–6539. [PubMed: 28815591]

Huganir RL, and Nicoll RA (2013). AMPARs and synaptic plasticity: the last 25 years. Neuron 80, 704–717. [PubMed: 24183021]

Izsvák Z, Fröhlich J, Grabundzija I, Shirley JR, Powell HM, Chapman KM, Ivics Z, and Hamra FK (2010). Generating knockout rats by transposon mutagenesis in spermatogonial stem cells. Nat. Methods 7, 443–445. [PubMed: 20473302]

Jackson AC, and Nicoll RA (2011). The expanding social network of ionotropic glutamate receptors: TARPs and other transmembrane auxiliary subunits. Neuron 70, 178–199. [PubMed: 21521608]

Jankowski MM, Ronnqvist KC, Tsanov M, Vann SD, Wright NF, Erichsen JT, Aggleton JP, and O'Mara SM (2013). The anterior thalamus provides a subcortical circuit supporting memory and spatial navigation. Front. Syst. Neurosci 7, 45. [PubMed: 24009563]

Kerrigan JF, Litt B, Fisher RS, Cranstoun S, French JA, Blum DE, Dichter M, Shetter A, Baltuch G, Jaggi J, et al. (2004). Electrical stimulation of the anterior nucleus of the thalamus for the treatment of intractable epilepsy. Epilepsia 45, 346–354. [PubMed: 15030497]

Keum S, and Marchuk DA (2009). A locus mapping to mouse chromosome 7 determines infarct volume in a mouse model of ischemic stroke. Circ. Cardiovasc. Genet 2, 591–598. [PubMed: 20031639]

Kielland A, and Heggelund P (2002). AMPA and NMDA currents show different short-term depression in the dorsal lateral geniculate nucleus of the rat. J. Physiol 542, 99–106. [PubMed: 12096054]

Klaassen RV, Stroeder J, Coussen F, Hafner AS, Petersen JD, Renancio C, Schmitz LJ, Normand E, Lodder JC, Rotaru DC, et al. (2016). Shisa6 traps AMPA receptors at postsynaptic sites and prevents their desensitization during synaptic activity. Nat. Commun 7, 10682. [PubMed: 26931375]

Lein ES, Hawrylycz MJ, Ao N, Ayres M, Bensinger A, Bernard A, Boe AF, Boguski MS, Brockway KS, Byrnes EJ, et al. (2007). Genome-wide atlas of gene expression in the adult mouse brain. Nature 445, 168–176. [PubMed: 17151600]

Mao X, Gu X, and Lu W (2017). GSG1L regulates the strength of AMPA receptor-mediated synaptic transmission but not AMPA receptor kinetics in hippocampal dentate granule neurons. J. Neurophysiol 117, 28–35. [PubMed: 27707810]

McGee TP, Bats C, Farrant M, and Cull-Candy SG (2015). Auxiliary Subunit GSG1L Acts to Suppress Calcium-Permeable AMPA Receptor Function. J. Neurosci 35, 16171–16179. [PubMed: 26658868]

Mirski MA, and Ferrendelli JA (1984). Interruption of the mammillothalamic tract prevents seizures in guinea pigs. Science 226, 72–74. [PubMed: 6433485]

Morel A, Magnin M, and Jeanmonod D (1997). Multiarchitectonic and stereotactic atlas of the human thalamus. J. Comp. Neurol 387, 588–630. [PubMed: 9373015]

Morrison RS, Wenzel HJ, Kinoshita Y, Robbins CA, Donehower LA, and Schwartzkroin PA (1996). Loss of the p53 tumor suppressor gene protects neurons from kainate-induced cell death. J. Neurosci 16, 1337–1345. [PubMed: 8778285]

Nakagawa T, Cheng Y, Ramm E, Sheng M, and Walz T (2005). Structure and different conformational states of native AMPA receptor complexes. Nature 433, 545–549. [PubMed: 15690046]

Narushima M, Uchigashima M, Yagasaki Y, Harada T, Nagumo Y, Uesaka N, Hashimoto K, Aiba A, Watanabe M, Miyata M, and Kano M (2016). The Metabotropic Glutamate Receptor Subtype 1 Mediates Experience-Dependent Maintenance of Mature Synaptic Connectivity in the Visual Thalamus. Neuron 91, 1097–1109. [PubMed: 27545713]

Oh SW, Harris JA, Ng L, Winslow B, Cain N, Mihalas S, Wang Q, Lau C, Kuan L, Henry AM, et al. (2014). A mesoscale connectome of the mouse brain. Nature 508, 207–214. [PubMed: 24695228]

Parker A, and Gaffan D (1997). The effect of anterior thalamic and cingulate cortex lesions on object-in-place memory in monkeys. Neuropsychologia 35, 1093–1102. [PubMed: 9256374]

Paz JT, and Huguenard JR (2015). Microcircuits and their interactions in epilepsy: is the focus out of focus? Nat. Neurosci 18, 351–359. [PubMed: 25710837]

Petrof I, and Sherman SM (2009). Synaptic properties of the mammillary and cortical afferents to the anterodorsal thalamic nucleus in the mouse. J. Neurosci 29, 7815–7819. [PubMed: 19535593]

Phillips JW, Schulmann A, Hara E, Winnubst J, Liu C, Valakh V, Wang L, Shields BC, Korff W, Chandrashekar J, et al. (2019). A repeated molecular architecture across thalamic pathways. Nat. Neurosci 22, 1925–1935. [PubMed: 31527803]

Rafols JA, and Valverde F (1973). The structure of the dorsal lateral geniculate nucleus in the mouse. A Golgi and electron microscopic study. J. Comp. Neurol 150, 303–332. [PubMed: 4124620]

Rodríguez CI, Buchholz F, Galloway J, Sequerra R, Kasper J, Ayala R, Stewart AF, and Dymecki SM (2000). High-efficiency deleter mice show that FLPe is an alternative to Cre-loxP. Nat. Genet 25, 139–140. [PubMed: 10835623]

Schwenk J, Harmel N, Zolles G, Bildl W, Kulik A, Heimrich B, Chisaka O, Jonas P, Schulte U, Fakler B, and Klöcker N (2009). Functional proteomics identify cornichon proteins as auxiliary subunits of AMPA receptors. Science 323, 1313–1319. [PubMed: 19265014]

Schwenk J, Harmel N, Brechet A, Zolles G, Berkefeld H, Müller CS, Bildl W, Baehrens D, Hüber B, Kulik A, et al. (2012). High-resolution proteomics unravel architecture and molecular diversity of native AMPA receptor complexes. Neuron 74, 621–633. [PubMed: 22632720]

Schwenk J, Baehrens D, Haupt A, Bildl W, Boudkkazi S, Roeper J, Fakler B, and Schulte U (2014). Regional diversity and developmental dynamics of the AMPA-receptor proteome in the mammalian brain. Neuron 84, 41–54. [PubMed: 25242221]

Shanks NF, Savas JN, Maruo T, Cais O, Hirao A, Oe S, Ghosh A, Noda Y, Greger IH, Yates JR 3rd, and Nakagawa T (2012). Differences in AMPA and kainate receptor interactomes facilitate identification of AMPA receptor auxiliary subunit GSG1L. Cell Rep. 1, 590–598. [PubMed: 22813734]

Sherman SM, and Guillery RW (2004). Thalamus In The Synaptic Organization of the Brain, Shepherd GM, ed. (Oxford University Press), pp. 311–359.

Shi W, Xianyu A, Han Z, Tang X, Li Z, Zhong H, Mao T, Huang K, and Shi SH (2017). Ontogenetic establishment of order-specific nuclear organization in the mammalian thalamus. Nat. Neurosci 20, 516–528. [PubMed: 28250409]

Staley K (2015). Molecular mechanisms of epilepsy. Nat. Neurosci 18, 367–372. [PubMed: 25710839]

Sun YG, and Beierlein M (2011). Receptor saturation controls short-term synaptic plasticity at corticothalamic synapses. J. Neurophysiol 105, 2319–2329. [PubMed: 21325678]

Takebayashi S, Hashizume K, Tanaka T, and Hodozuka A (2007). The effect of electrical stimulation and lesioning of the anterior thalamic nucleus on kainic acid-induced focal cortical seizure status in rats. Epilepsia 48, 348–358. [PubMed: 17295630]

Tomita S, Chen L, Kawasaki Y, Petralia RS, Wenthold RJ, Nicoll RA, and Bredt DS (2003). Functional studies and distribution define a family of transmembrane AMPA receptor regulatory proteins. J. Cell Biol 161, 805–816. [PubMed: 12771129]

Traynelis SF, Wollmuth LP, McBain CJ, Menniti FS, Vance KM, Ogden KK, Hansen KB, Yuan H, Myers SJ, and Dingledine R (2010). Glutamate receptor ion channels: structure, regulation, and function. Pharmacol. Rev 62, 405–496. [PubMed: 20716669]

Twomey EC, Yelshanskaya MV, Grassucci RA, Frank J, and Sobolevsky AI (2016). Elucidation of AMPA receptor-stargazin complexes by cryo-electron microscopy. Science 353, 83–86. [PubMed: 27365450]

Twomey EC, Yelshanskaya MV, Grassucci RA, Frank J, and Sobolevsky AI (2017a). Channel opening and gating mechanism in AMPA-subtype glutamate receptors. Nature 549, 60–65. [PubMed: 28737760]

Twomey EC, Yelshanskaya MV, Grassucci RA, Frank J, and Sobolevsky AI (2017b). Structural Bases of Desensitization in AMPA Receptor-Auxiliary Subunit Complexes. Neuron 94, 569–580. [PubMed: 28472657]

von Engelhardt J, Mack V, Sprengel R, Kavenstock N, Li KW, Stern-Bach Y, Smit AB, Seeburg PH, and Monyer H (2010). CKAMP44: a brain-specific protein attenuating short-term synaptic plasticity in the dentate gyrus. Science 327, 1518–1522. [PubMed: 20185686]

Willems J, de Jong APH, Scheefhals N, Mertens E, Catsburg LAE, Poorthuis RB, de Winter F, Verhaagen J, Meye FJ, and MacGillavry HD (2020). ORANGE: A CRISPR/Cas9-based genome

editing toolbox for epitope tagging of endogenous proteins in neurons. PLoS Biol. 18, e3000665. [PubMed: 32275651]

Wolff M, Gibb SJ, and Dalrymple-Alford JC (2006). Beyond spatial memory: the anterior thalamus and memory for the temporal order of a sequence of odor cues. J. Neurosci 26, 2907–2913. [PubMed: 16540567]

Wright NF, Erichsen JT, Vann SD, O'Mara SM, and Aggleton JP (2010). Parallel but separate inputs from limbic cortices to the mammillary bodies and anterior thalamic nuclei in the rat. J. Comp. Neurol 518, 2334–2354. [PubMed: 20437531]

Wu G, Lu ZH, Wang J, Wang Y, Xie X, Meyenhofer MF, and Ledeen RW (2005). Enhanced susceptibility to kainate-induced seizures, neuronal apoptosis, and death in mice lacking gangliotetraose gangliosides: protection with LIGA 20, a membrane-permeant analog of GM1. J. Neurosci 25, 11014–11022. [PubMed: 16306414]

Zhao Y, Chen S, Swensen AC, Qian WJ, and Gouaux E (2019). Architecture and subunit arrangement of native AMPA receptors elucidated by cryo-EM. Science 364, 355–362. [PubMed: 30975770]

Zheng Y, Mellem JE, Brockie PJ, Madsen DM, and Maricq AV (2004). SOL-1 is a CUB-domain protein required for GLR-1 glutamate receptor function in C. elegans. Nature 427, 451–457. [PubMed: 14749834]

Highlights

- Input-specific synaptic phenotypes in the anterior thalamic neurons of GSG1L KO mice
- Short-term plasticity in corticothalamic synapses is regulated by GSG1L
- Stargazin is functionally absent from corticothalamic synapses
- GSG1L KO mice have increased hyperexcitability and seizure susceptibility

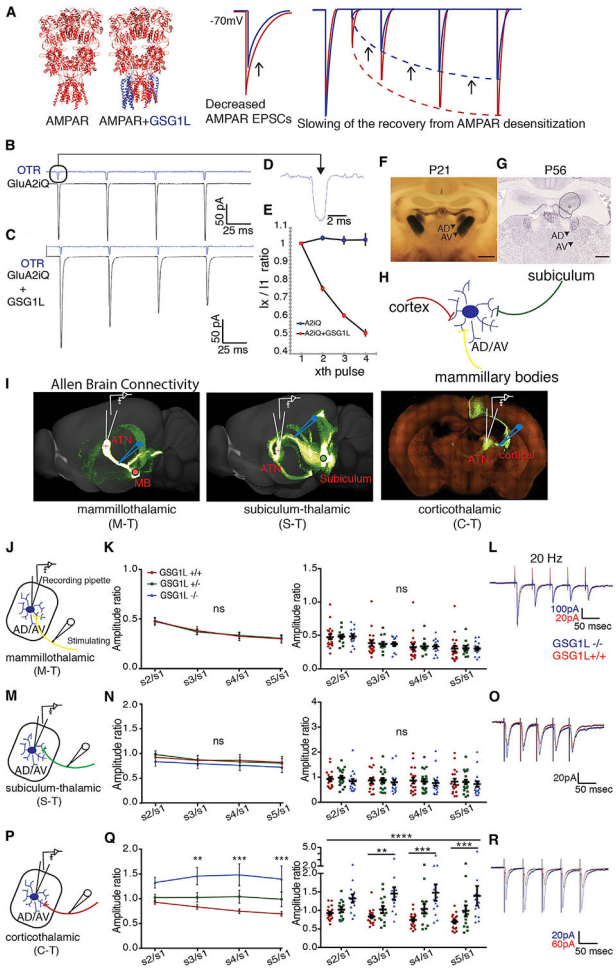

Figure 1. GSG1L Input Specifically Regulates Short-Term Plasticity at AD/AV

(A) Ribbon diagram of GluA2 (red) with or without GSG1L (blue) (PDB: 5WEK) (Twomey et al., 2017a). Schematic summarizing the effects of GSG1L, emphasized with black arrows (right). AMPAR+GSG1L (blue lines) exhibits decreased amplitude and slower recovery from desensitization compared with AMPAR alone (red lines).

(B–E) Recordings from outside-out patches. Representative averaged traces for (B) GluA2iQ (i.e., flip/Q pore) alone and (C) GluA2iQ+GSG1L. OTR, open tip response. (D) Magnified view of the OTR. (E) Ratio of each pulse over the first pulse (Ix/I1, where x = 2, 3, and 4). A2iQ (n = 5), A2iQ+GSG1L (n = 4) ($p < 0.001$ for pulses 2–4, two-way ANOVA).

(F) GSG1L KO rat brain coronal sections at P21 (scale bar, 1,000 μm). The lacZ expression is represented by dark blue stain (arrowheads show AD/AV).

(G) *In situ* hybridization data from the Allen Brain Atlas. The lower signal intensity in AV reflects lower cell density in AV compared with AD (Morel et al., 1997); see also Figure S1E.

(H) Inputs received by AD/AV.

(I) Input-dependent stimulation paradigm of AD/AV (scale bar, 420 μm). Brain images were derived from Allen brain connectivity (scale bar, 1,000 μm) (Oh et al., 2014).

(J, M, and P) Schematic of mammilothalamic, M-T pathway (J), subiculum-thalamic, S-T pathway (M), and corticothalamic, C-T pathway (P).

(K) Pulse ratios of electrically evoked EPSCs from AD/AV neurons at a holding potential of −70 mV of GSG1L KO (P21–P33, n = 15 cells, N = 6 mice), Het (n = 13, N = 5), and WT (n = 20, N = 8). S1–S5 are amplitudes of each stimulus in a train of five stimuli ($p = 0.9956$, two-way ANOVA). S(n)/S1, where n = 2, …, 5, is the paired-pulse ratio of the 2^{nd}–5^{th} pulse divided by the 1^{st} pulse. (L, O, and R) Superimposed sample traces of whole-cell recordings of currents in AD/AV in response to stimulating M-T (L), S-T (O), or C-T (R) pathway.

(N) No changes in pulse ratios of GSG1L KO (P21–P33, n = 18, N = 6), Het (n = 20, N = 6), and WT (n = 18, N = 7) ($p = 0.7288$, two-way ANOVA) in response to subiculum stimulation at 20 Hz.

(Q) Pulse ratios are significantly different for GSG1L KO (P21–P33, n = 13, N = 6), Het (n = 14, N = 6), and WT (n = 19, N = 7) at 20 Hz ($p < 0.0001$, two-way ANOVA) in response to cortical stimulation. *Post hoc* Sidak comparisons: **$p < 0.01$, ***$p < 0.001$, ****$p < 0.0001$.

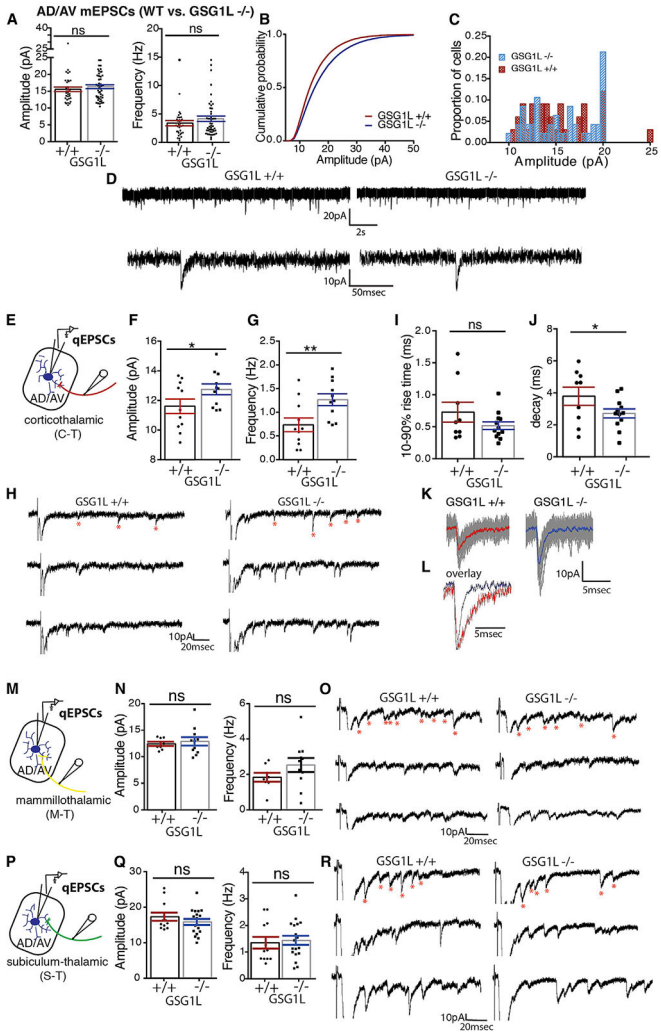

Figure 2. GSG1L Is a Negative AMPAR Regulator at C-T Synapses in AD/AV

(A) Mean amplitude and frequency of AMPAR-mediated mEPSCs in AD/AV of GSG1L KO and GSG1L WT ($p = 0.3082$, $p = 0.4054$, respectively, Mann-Whitney U test). GSG1L KO (P15–P30, n = 47, N = 4); GSG1L WT (n = 33, N = 3).

(B) Cumulative plot of the amplitude distribution ($p = 0.0041$, Kolmogorov-Smirnov [K-S] test).

(C) Histogram of amplitudes of individual cells.

(D) Representative traces of AMPAR-mediated mEPSCs in each genotype.

(E, M, and P) Asynchronous qEPSCs recorded at C-T (E), M-T (M), or S-T (P) synapses at AD/AV in GSG1L WT and KO.

(F and G) Amplitude (P15–P30, $p = 0.0378$, Mann-Whitney U test) (F) and frequency (G) of qEPSCs ($p = 0.0060$, Mann-Whitney U test) comparing GSG1L KO (n = 11, N = 4) and WT (n = 11, N = 5).

(H) Representative traces of qEPSCs.

(I and J) Pooled data for rise time ($p = 0.0900$, Mann-Whitney U test) (I) and decay kinetics ($p = 0.0413$, Mann-Whitney U test) (J). Each data point is an average obtained from one neuron.

(K) Representative traces of averaged qEPSCs from one neuron in GSG1L WT (red) and KO (blue). Raw traces are shown in gray.
(L) Averaged qEPSCs in (K) are normalized and overlaid for comparison.
(N) Amplitude ($p = 0.4455$, Mann-Whitney U test) and frequency ($p = 0.0535$, Mann-Whitney U test) of M-T qEPSCs comparing GSG1L KO ($n = 11$, $N = 5$) and WT ($n = 8$, $N = 6$).
(O and R) Representative traces of qEPSCs from the M-T pathway (O) and S-T pathway (R) in GSG1L WT and KO.
(Q) Amplitude ($p = 0.2184$, Mann-Whitney U test) and frequency ($p = 0.3269$, Mann-Whitney U test) of S-T qEPSCs of GSG1L KO ($n = 18$, $N = 5$) and WT ($n = 12$, $N = 6$).

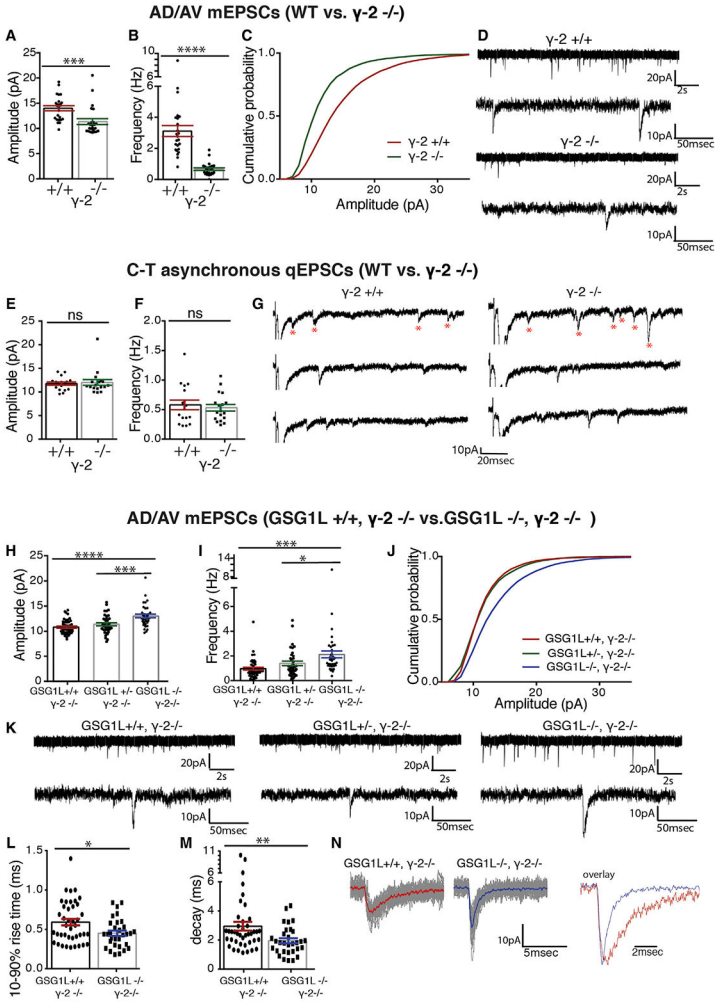

Figure 3. GSG1L Is a Dominant Auxiliary Subunit at C-T Synapses at AD/AV

(A) Mean amplitude of AMPAR-mediated mEPSCs in AD/AV of γ−2 KO and γ−2 WT (p = 0.0006, Mann-Whitney U test). γ−2 KO (P15–P22, n = 24, N = 3); γ−2 WT (n = 24, N = 3).

(B) Frequency of mEPSCs (p < 0.0001, Mann-Whitney U test).

(C) Cumulative plot of the amplitude distribution between γ−2 KO and WT animals (p = 0.024, K-S test).

(D) Representative AMPAR-mediated mEPSC traces of AD/AV neurons.

(E and F) Asynchronous qEPSCs recorded at C-T synapses at AD/AV in γ−2 WT (P15–P22, n = 17, N = 6) and KO (n = 18, N = 6). Mean amplitude (p = 0.4123, Mann-Whitney U test) (E) and frequency (p = 0.4578, Mann-Whitney U test) (F) of qEPSCs.

(G) Representative traces of qEPSCs at C-T synapses.

(H) Mean amplitude of AMPAR-mediated mEPSCs in AD/AV of GSG1L KO/γ−2 KO mice relative to the GSG1L WT/γ−2 KO and GSG1L Het/γ−2 KO (P15–P22, p < 0.0001, two-way ANOVA). GSG1L WT/γ−2 KO (n = 45, N = 6); GSG1L HET/γ−2 KO (n = 37, N = 5); GSG1L KO/γ−2 KO (n = 36, N = 5).

(I) Frequency of mEPSCs (p = 0.0003, two-way ANOVA).

(J) Cumulative plot showing amplitude distribution (p = 0.0166, K-S test).

(K) Representative AMPAR-mediated mEPSC traces from corresponding genotypes.
(L and M) Rise time ($p = 0.0277$, Mann-Whitney U test) (L) and decay time ($p = 0.0058$, Mann-Whitney U test) (M) of mEPSCs in GSG1L KO/γ−2 KO (blue) relative to GSG1L WT/γ−2 KO (red).
(N) Representative traces of averaged mEPSCs, with the averages shown in bold. The averages of individual mEPSCs are normalized and overlaid for comparison with GSG1L KO/γ−2 KO in blue and GSG1L WT/γ−2 KO in red. *Post hoc* Sidak comparisons: *$p < 0.05$, ***$p < 0.001$, ****$p < 0.0001$.

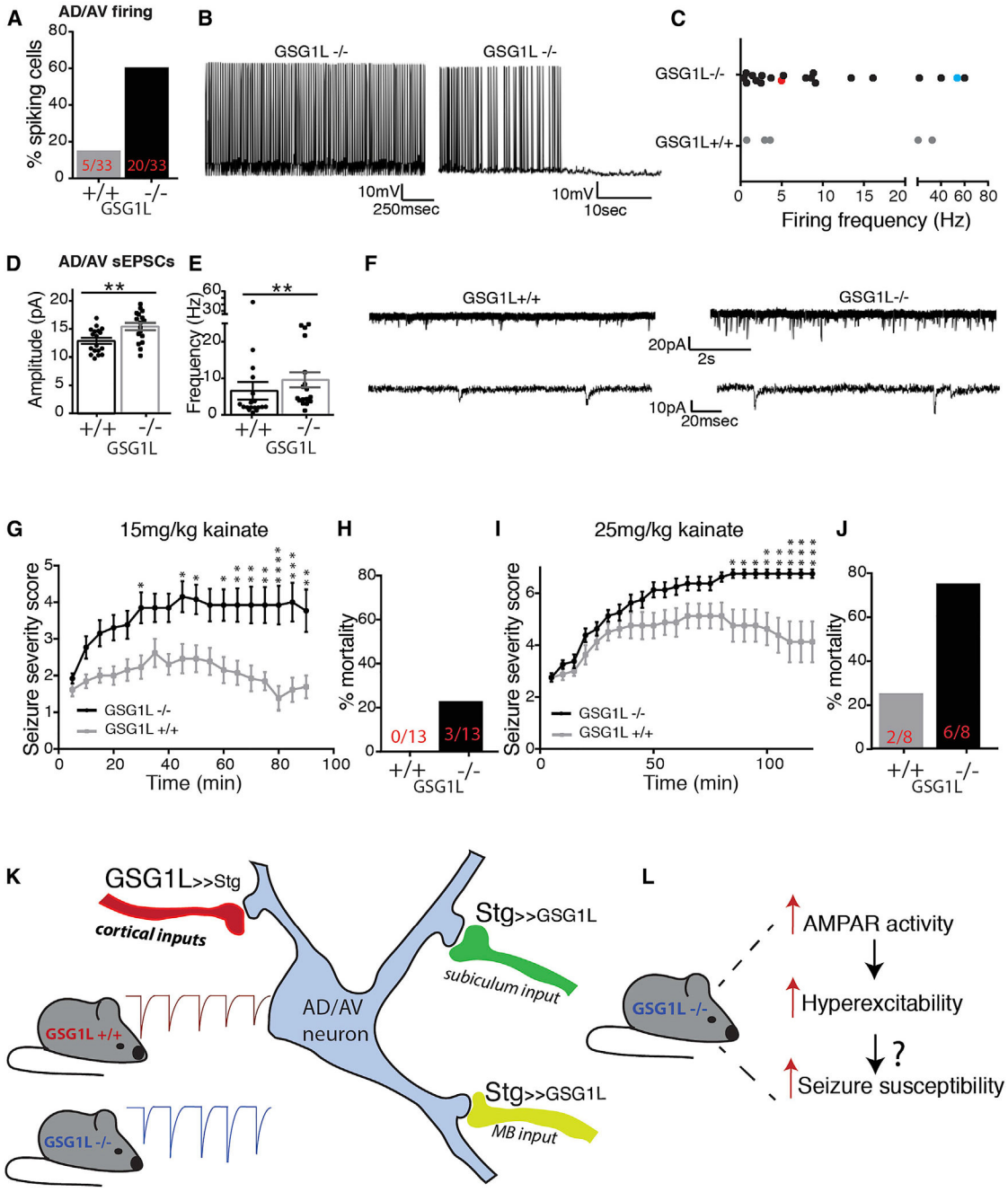

Figure 4. Loss of GSG1L Results in Enhanced Excitability and Seizure Susceptibility

(A) Bar graph summarizing spontaneously firing AD/AV neurons in GSG1L KO (20/33 cells, N = 5) and WT control (5/33 cells, N = 5).

(B) Representative traces of two spiking GSG1L KO AD/AV neurons.

(C) Bar graph summarizing firing frequency distribution. Blue and red data points represent left and right traces in (B), respectively.

(D and E) Mean amplitude (p = 0.0037, Mann-Whitney U test) and frequency (p = 0.0084, Mann-Whitney U test) of AMPAR-mediated sEPSCs in AD/AV neurons of GSG1L KO (P15–P30, n = 17, N = 4) and WT (n = 18, N = 4).

(F) Representative sEPSC traces of GSG1L KO and WT.

(G–J) Time course of seizure severity following i.p. injection of 15 mg/kg (n = 13 each, 9–10 months) (G) or 25 mg/kg (n = 8 each) (I) of kainate. A higher score corresponds to a severer seizure status, with 7 denoting death. (H and J) Mortality rate during the 2-h recording period at 15 mg/kg (H) and 25 mg/kg (J) injection. Two-way ANOVA, $p < 0.0001$ for both doses. *Post hoc* Sidak comparisons: *$p < 0.05$, **$p < 0.01$, ***$p < 0.001$, ****$p < 0.0001$.

(K and L) Summary schema. (K) GSG1L is a dominant auxiliary subunit in C-T synapses (red) of AD/AV neurons (blue). In these synapses, GSG1L suppresses short-term facilitation by slowing recovery from AMPAR desensitization. γ−2 (Stg) is a dominant auxiliary subunit in S-T synapses (green) and M-T synapses (yellow) in AD/AV. (L) Consistent with GSG1L being a negative regulator of AMPARs, GSG1L KO mice have increased AMPAR-mediated quantal events in C-T synapses. GSG1L KO mice have enhanced excitability in the AT. The enhanced hyperexcitability is accompanied by increased susceptibility to kainate-induced seizures in GSG1L KO mice.

KEY RESOURCES TABLE

REAGENT or RESOURCE	SOURCE	IDENTIFIER
Antibodies		
Anti-GSG1L Ct-1 anitbody	(Shanks et al., 2012)	PMID: 22813734
Anti-GSG1L Ct-2 antibody	(Shanks et al., 2012)	PMID: 22813734
Anti-GluA2CT antibody	(Nakagawa et al., 2005)	PMID: 15690046
Pan-TARP antibody	(Nakagawa et al., 2005)	PMID: 15690046
Anti-Stargazin antibody	Millipore	AB9876; RRID: AB_877307
Chemicals, Peptides, and Recombinant Proteins		
Picrotoxin	Tocris	1128
Tetrodotoxin Citrate	Abcam	Ab120055
Cyclothiazide	Tocris	0713
Kainic acid monohydrate	Sigma	K0250
NBQX	Tocris	1044
Experimental Models: Organisms/Strains, Cell lines		
Mouse: GSG1L −/−	This paper	N/A
Mouse: CACNG2 −/−	This paper	N/A
Mouse: GSG1L −/− / CACNG2 −/−	This paper	N/A
Rat: GSG1L −/−	(Izsvák et al., 2010)	PMID: 21193047
TetON HEK cells	Clontech	631182
Oligonucleotides		
Genotyping Primer GSG1L, mouse, left: aaacagacaacatggccctcagactc	Sigma	N/A
Genotyping Primer GSG1L, mouse right: gacttgtcccatctctaggatacctccc	Sigma	N/A
Genotyping Primer GSG1L, rat, left: acgttgtagtgaccccaagc	Sigma	N/A
Genotyping Primer GSG1L, rat, right: tgcacgcatactacaatga	Sigma	N/A
Genotyping Primer CACNG2, mouse, left: atggtgttgagaattcggctgtacc	Sigma	N/A
Genotyping Primer CACNG2, mouse, right: aaccctaaggactccaaagcatcc	Sigma	N/A
Recombinant DNA		
DualpTREt-GluA2i(Q)+GSG1L	This paper	N/A
GluA2i(Q)	(Hawken et al., 2017)	N/A
Software and Algorithms		
Prism 6.0	Graphpad Software	https://www.graphpad.com/scientific-software/prism/
PCLAMP10	Molecular Devices	https://www.moleculardevices.com/products/axon-patch-clamp-system/acquisition-and-analysis-software/pclamp-software-suite
IGOR Pro	WaveMetrics	https://www.wavemetrics.com/products/igorpro
Neuromatics	WaveMetrics	http://www.neuromatic.thinkrandom.com/index.html
LabView	National Instruments	https://www.ni.com/en-us/shop/labview/labview-details.html

REAGENT or RESOURCE	SOURCE	IDENTIFIER
Adobe Illustrator 2020	Adobe	https://www.adobe.com/products/illustrator.html